Self-Localization and 3-D Model Construction of Pipe by Earthworm Robot Equipped with Omni-Directional Rangefinder

Atsushi Yamashita, Kenki Matsui, Ryosuke Kawanishi, Toru Kaneko
Taro Murakami, Hayato Omori, Taro Nakamura and Hajime Asama

Abstract— A lot of plumbings such as gas pipes and water pipes exist in public utilities, factories and so on. The use of an omni-directional camera which can take images of 360 deg in surroundings at a time is effective for pipe inspection. However, shape measurement is difficult only with the omni-directional camera. Therefore, in this paper, we propose a reconstruction method of a piping shape by using a rangefinder constructed with an omni-directional camera and an omni-directional laser. The rangefinder is mounted on an earthworm robot. Our method calculates 3-D coordinates by the light section method. By integrating the 3-D coordinates with the information of camera motion estimated by the structure from motion technique, the shape of the pipe is reconstructed. The validity of the proposed method is shown through experiments.
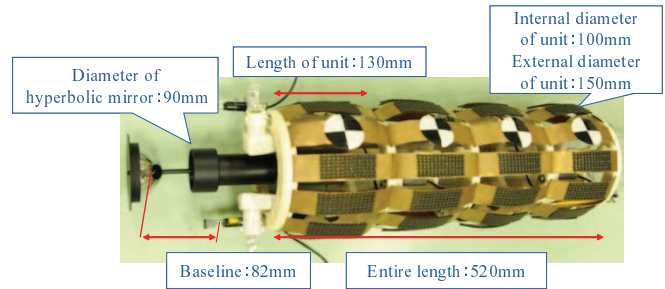
Fig. 1. Earthworm robot equipped with omni-directional rangefinder.

I. INTRODUCTION

In this paper, we propose a self-localization method of an earthworm robot equipped with an omni-directional rangefinder (Fig. 1) and 3-D model construction method of pipes.

A lot of plumbings such as gas pipes and water pipes exist in public utilities, factories, power plants and so on. These facilities are important and indispensable for our lives. However, these pipes become deteriorated by aging and internal damage comes to existence. If the damage grows large, a serious accident may happen. To find such damage at the early stage, and to take precautions against possible accidents, it is important to recognize the pipe state.

It is difficult for humans to inspect the pipe state directly because they are long and narrow, and often lie underground. Therefore, automated inspection by robots equipped with camera is desirable and many efforts have been done to solve the problem [1]–[5].

However, most of existing inspection robots must rotate the camera to record images in piping because a conventional camera with a narrow view can see only one direction while piping has a cylindrical geometry. There is a problem that the inspection robot has to stop every time at the point where the robot records the image. Therefore, it takes long time to measure pipe shape.

On the other hand, vision sensors with a wide field of view have been proposed; e.g. a fisheye camera and an omni-directional camera. They have a variety of potential applications, such as mobile robot navigation [6], and teleprese̶nse technology [7]. Particularly, previous studies showed that an omni-directional camera is effective in measurement and recognition of environment [8].

Kannala *et al.* proposed a pipe inspection method using an omni-directional vision sensor [9]. The use of the omni-directional vision sensor that can take images of 360 deg in surrounding at a time is effective for pipe inspection. They use structure from motion (SFM) which is a kind of passive measurement. However, the method has to extract and track feature points to get corresponding points between images. If corresponding point detection fails, the measurement accuracy decreases.

To solve this problem, a light section method which is a kind of active measurement is proposed instead of passive measurement like SFM. The light section method has an advantage that the method usually has no difficulty in finding corresponding points. Therefore, measurement is more reliable than SFM and the method is used in various fields.

However, in general, the light section method requires that the position and the orientation of the camera are fixed while measurement. If the camera moves, it is difficult to integrate the measurement results. Therefore, the camera motion estimation (the relative relations of camera positions and orientations) is important for the measurement.

The idea of light section method with an omni-directional camera can be found in works such as [10]–[13]. However, Kurisu *et al.*, Senoh *et al.*, and Yi *et al.* do not describe

Atsushi Yamashita and Hajime Asama are with Department of Precision Engineering, The University of Tokyo, 7-3-1 Hongo, Bunkyo-ku, Tokyo 113-8656, Japan
(e-mail: {yamashita, asama}@robot.t.u-tokyo.ac.jp)
Kenki Matsui, Ryosuke Kawanishi and Toru Kaneko are with Department of Mechanical Engineering, Faculty of Engineering, Shizuoka University, 3-5-1 Johoku, Naka-ku, Hamamatsu-shi, Shizuoka 432-8561, Japan
Taro Murakami, Hayato Omori and Taro Nakamura are with Department of Precision Mechanics, Chuo University, 1-13-27 Kasuga, Bunkyo-ku, Tokyo 112-8551, Japan (e-mail: nakamura@mech.chuo-u.ac.jp)

camera motion estimation. Orghidan *et al.* proposes a camera motion estimation method based on ICP algorithm. However, the method is difficult to estimate 6DOF motion of the camera.

On the other hand, SFM has the advantage that it can estimate the camera motion with 3-D measurement. The method is used not only for pipe inspection but also for construction of an environment map [14]–[16].

We have already proposed a reconstruction method of pipe shape with a light section method and SFM by using omni-directional range finder [17]. However, there are some problems.

First, we have not mounted the range finder to a pipe inspection robot. A lot of pipe inspection robots are proposed as mentioned above. Especially, the robot that imitates the earthworm is actively developed [18], [19]. The earthworm type robot is suitable for movement in the piping, because the ground contact area with piping is large.

Second, the baseline between the omni-directional camera and the laser source was not optimized. The decision of the baseline is important to improve the measurement accuracy.

Third, the distortion of the omni-directional image was not considered. The measurement accuracy can be improved by removing the distortion.

In this paper, we propose an omni-directional range finder that solves the above-mentioned three problems.

II. Outline

An inspection robot executes measurement by using a rangefinder constructed with an omni-directional camera (Fig. 2) and a laser source that can emit laser light in all direction orthogonal to the head (Fig. 3).

As an inspection robot, we use an earthworm robot. The earthworm propagates a longitudinal wave from the anterior to posterior part using contraction muscles in consecutive segments. The locomotion pattern can be described as follows:

(1) The anterior segments of the earthworm are contracted by the longitudinal muscle.

(2) The contraction continuously propagates to the rear end.

(3) The anterior segments of the earthworm are extended in the axial direction by the circular muscle. Since the friction between the segments and the moving surface is reduced, thinner segments can move smoothly.

(4) The extended segments continuously propagate in the rear direction. The forward segments are pushed in the direction of movement.

We developed an earthworm robot by referring to an actual motion of earthworm. (Fig. 4) [19]. A unit of the robot is equal to a segment of an actual earthworm. Each of them can extend and contract in the axial direction, which is necessary to realize peristaltic crawling.

The process of our method is shown in Fig. 5. As the first step, the inspection robot acquires an omni-directional image sequence during its locomotion while emitting laser light.

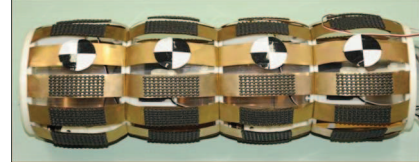Fig. 2.   Omni-directionalcamera.

Fig. 3.   Omni-directional laser.

Fig. 4.   Earthworm robot [19].

.

The second step calculates 3-D coordinates of measurement points by the light section method.

The third step estimates a camera motion by SFM and integrates measurement results.

Finally, a triangular mesh is generated from the measurement results. By texture mapping to the triangular mesh, the 3-D model of pipe is reconstructed.

III. 3-D Measurement

We use the light section method for 3-D measurement. First, we extract image coordinates of laser light from an omni-directional image sequence. Then, the 3-D coordinates of measurement point are given as the cross-point of a ray vector and the laser light.

A. Laser Light Extraction

The laser light reflected by the measurement object is captured by the omni-directional camera as a circular area with some width. Therefore, we have to extract the peak (the pixel that has the highest intensity) from the area that can be considered as the laser light on the image. We use the Gaussian approximation method [20] to extract the peak.

B. 3-D Coordinates Calculation

We define a unit vector which starts at the center of projection and ends at a measurement point in 3-D space as a ray vector $\mathbf{r} = [x, y, z]^T$, where T stands for transposition of a vector.

The omni-directional camera has a hyperboloid mirror in front of lens of a conventional camera. Therefore, as shown in Fig. 6, ray vector $\mathbf{r}$ is directed from the focus of the hyperboloid mirror to the reflection point of the ray on the mirror surface.

Ray vector $\mathbf{r}$ is calculated from image coordinates $[u, v]$ of the laser light using Eq. (1).

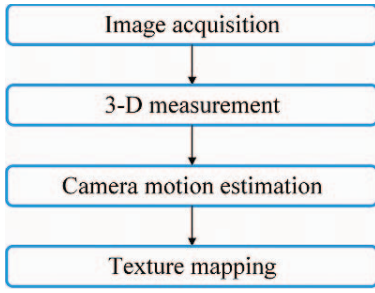$$\mathbf{r} = \lambda \begin{pmatrix} su \\ sv \\ sf - 2c \end{pmatrix}, \tag{1}$$

Fig. 5.   Procedure.
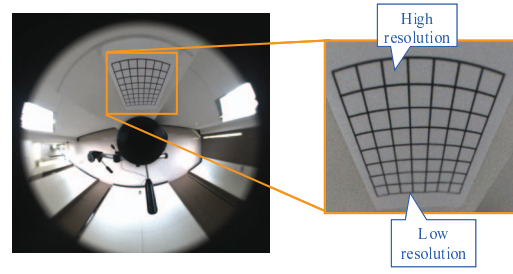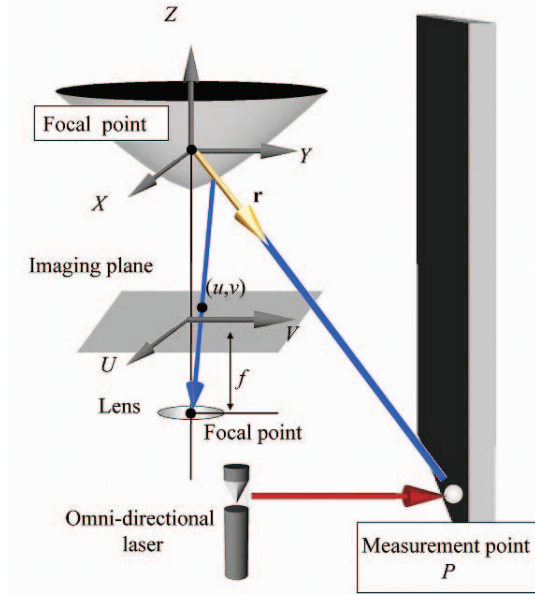

Fig. 7.   Resolution of omni-directional image.

Fig. 6.   Calculation of 3-D coordinates.

IV. OPTIMIZATION OF BASELINE

The distance between the omni-directional camera and the laser source (baseline length) is important for the improvement of measurement accuracy. Therefore, we decide the baseline to minimize the measurement error.

Figure 7 shows the image resolution of an omni-directional camera. The resolution of the center part of the image is low, because the pixel count of the center part of the image is fewer than that of the outer part of the image. Therefore, it is an unsuitable area for measurement from a viewpoint of the resolution. The analysis for optimizing the baseline is made based on above.

Generally, accuracy of stereo measurement depends on the baseline length. In our proposed method, however, the image formation position changes to the center part of the image as the baseline expands (Fig. 8). Therefore, the relation of the trade-off exists between the baseline and the resolution.

The baseline is optimized by calculating the measurement error in each baseline.

Suppose that the effective number of pixels of the CCD camera is $p_H \times p_V$ [pixels], the size of each pixel is $s_H \times s_V$ [mm], and the size of the captured image is $H \times V$ [pixels]. The relation between the baseline l and the measurement error Δd in the depth direction is calculated using Eqs. (6)-(9).

where

$$c = \sqrt{a^2 + b^2}, \quad (2)$$

$$s = \frac{a^2(f\sqrt{a^2+b^2} + b\sqrt{u^2+v^2+f^2})}{a^2 f^2 - b^2(u^2+v^2)}. \quad (3)$$

In these equations, a, b, and c are the hyperboloid parameters, and f is the image distance (the distance between the center of the lens and the image plane) of camera. λ represents the scale of a ray vector.

Then, we define the plane of laser light as Eq. (4). In the equation, k_1, k_2, k_3, k_4 are the planar parameters calibrated in advance.

$$k_1 x + k_2 y + k_3 z + k_4 = 0. \quad (4)$$

From Eqs. (1)-(4), the 3-D coordinates of the measurement point is calculated by Eq. (5).

$$\begin{pmatrix} x_p \\ y_p \\ z_p \end{pmatrix} = \frac{-k_4}{k_1 su + k_2 sv + k_3(sf - 2c)} \begin{pmatrix} su \\ sv \\ sf - 2c \end{pmatrix}. \quad (5)$$

$$\Delta d = \frac{(c^2 - b^2)((b^2+c^2)\sqrt{f^2+r^2}f - 2bcf^2)\Delta r}{\sqrt{f^2+r^2}(b^2+c^2)f - 2bc\sqrt{f^2+r^2}} l, \quad (6)$$

$$r = fa \frac{\frac{cl}{d} + b\sqrt{1+(\frac{l}{d})^2}}{b\sqrt{\frac{cl}{d} + b\sqrt{1+(\frac{l}{d})^2} + a^2 \kappa^2} + ac\kappa}, \quad (7)$$

$$\kappa = \left(\frac{b}{a} + \frac{l}{d}\right)\left(\frac{b}{a} - \frac{l}{d}\right), \quad (8)$$

$$\Delta r = \sqrt{\left(\frac{1}{2}\frac{p_H s_H}{H}\right)^2 + \left(\frac{1}{2}\frac{p_V s_V}{V}\right)^2}. \quad (9)$$

In these equations, d is the distance to measurement object, r is the distance from image center to laser light, and Δr is the quantization error on the image plane, respectively.

Figure 9 shows the relation between the error rate $\Delta d/d$ and l with several values of d. The smaller the error rate is, the smaller the measurement error becomes.

From Fig. 9, there is an optimal l that minimizes the error rate for any given d. Therefore, if d is specified, the optimal
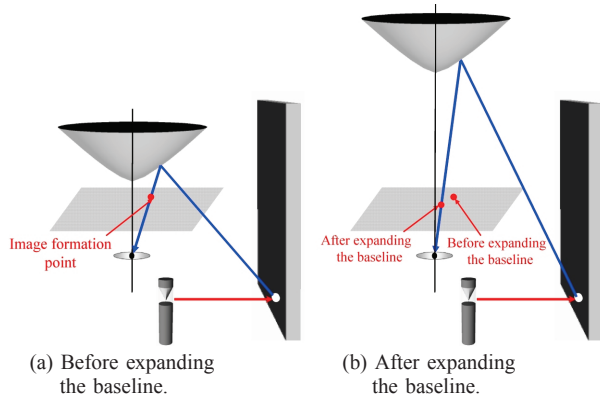
(a) Before expanding the baseline. (b) After expanding the baseline.

Fig. 8.   Change of image formation position.
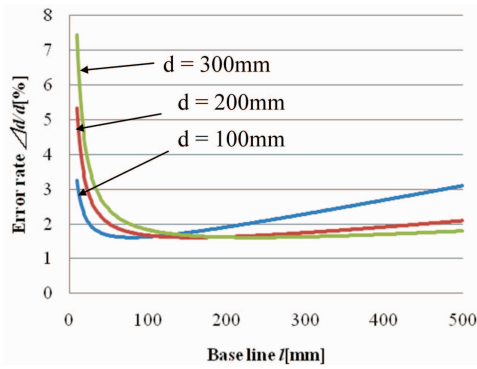
Fig. 9.   Relation between baseline and measurement error.

Fig. 10.   Procedure of SFM.

l can be decided. The optimal l is 82mm when d is 100mm. Also, l is 156mm when d is 200mm and l is 235mm when d is 300mm.

V.   Camera Motion Estimation

We use SFM for camera motion estimation (Fig. 10).

First, the robot acquires an omni-directional image sequence during its locomotion.

Second, the method extracts and tracks feature points to get corresponding points in the omni-directional image sequence.

The camera motion is estimated first by the linear estimation, which uses the positions of corresponding points in two images taken at each observation point.

In order to estimate the camera motion more precisely, re-estimation of camera motion is performed with nonlinear estimation.

A. Corresponding Point Acquisition

For getting corresponding points between images in the omni-directional image sequence, the method extracts feature points in the first image and then tracks them along the image sequence. In our method, SIFT (Scale Invariant Feature Transform) algorithm [21] is used.

However, the distortion of the omni-directional image and the projection distortion disturb correspondence point acquisition.
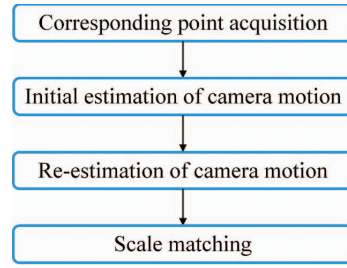
The perspective projection conversion is used to solve this problem. The omni-directional camera with a hyperboloid mirror can convert the omni-directional image to the perspective projection image (Fig. 11). The perspective projection image is generated by projecting the omni-directional image to the projection plane in the 3-D space.

Calculation of the projection plane is important for the decrease of the various distortions. When the projection plane leans, the projection distortion arises to the perspective projection image (Fig. 12). The error of SIFT features becomes small if the distortion is small when the SIFT features are compared. Therefore, we search for the center position and the gradient of the projection plane that minimizes SIFT features as follows. Corresponding points are acquired from the perspective projection image calculated based on the center position and the gradient.

Let $\mathbf{d}$ be the center position of the projection plane and $\mathbf{s_x}$ and $\mathbf{s_y}$ be the axis of the projection plane.

At first, the method calculates $\mathbf{d}$. As the first step, our method acquires images taken before and after the camera movement. Then, feature points are extracts from the after image by the SIFT method. Ray vector $\mathbf{r_1}$ is calculated from these feature points. The epipolar line in the before image is calculated from $\mathbf{r_1}$ and the information of camera motion. $\mathbf{d}$ is given by searching along the epipolar line of the $\mathbf{r_1}$ in the before image (Fig. 13).

In the next step, the ray vector $\mathbf{r_2}$ that passes each point on the epipolar line is calculated. The candidate point of $\mathbf{d}$ is calculated as cross point of $\mathbf{r_1}$ and each $\mathbf{r_2}$.

In the third step, the projection plane is generated centering on each $\mathbf{d}$. An omni-directional image is enlarged on the projection plane. And the projection plane is projected to the image plane.

After these steps, the before image and the after image are converted to the perspective projection image at each candidate point of $\mathbf{d}$. By comparing SIFT features between these images, $\mathbf{d}$ which minimizes the error of SIFT features is decided.

Then, $\mathbf{s_x}$ and $\mathbf{s_y}$ are rotated at the position of $\mathbf{d}$. SIFT features are compared while rotating $\mathbf{s_x}$ and $\mathbf{s_y}$. At last, corresponding points which are regarded as the same point in 3-D space can be obtained.

Here, the information of the camera motion is necessary for calculating the epipolar line. Therefore, our method estimates initial value of camera motion without considering
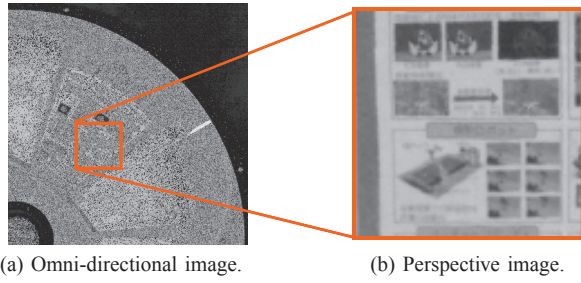
(a) Omni-directional image.   (b) Perspective image.

Fig. 11.   Perspective translation.

Fig. 12.   Projective distortion.

Fig. 13.   Detection of corresponding point.

Fig. 14.   Estimation of camera motion.
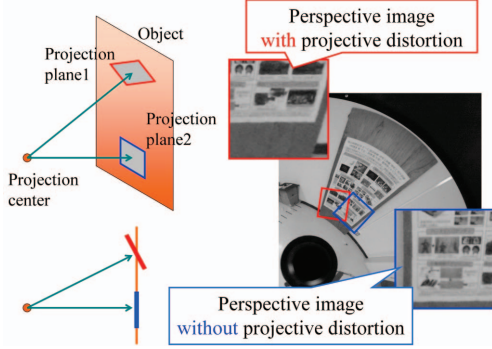
image distortion. By using the initial value, corresponding points are obtained by the method described in this chapter. Then, the camera motion is estimated again.

B. Estimation of Camera Motion

The camera motion is estimated by the eight-point algorithm [22].

In order to estimate camera motion, we calculate the essential matrix which contains information about relative position and orientation differences between two observation points.

Essential Matrix E satisfies Eq. (10).

$$\mathbf{r}_i'^T \mathbf{E} \mathbf{r}_i = 0, \tag{10}$$

where $\mathbf{r}_i = [x_i, y_i, z_i]^T$, $\mathbf{r}'_i = [x'_i, y'_i, z'_i]^T$ are the ray vectors of the corresponding point in two images, respectively (Fig. 14). Equation (10) is transformed into Eq. (11).

$$\mathbf{u}_i^T \mathbf{e}_i = 0, \tag{11}$$

where

$$\mathbf{u}_i = [x_i x'_i, y_i x'_i, z_i x'_i, x_i y'_i, y_i y'_i, z_i y'_i, x_i z'_i, y_i z'_i, z_i z'_i]^T, \tag{12}$$
$$\mathbf{e} = [e_{11}, e_{12}, e_{13}, e_{21}, e_{22}, e_{23}, e_{31}, e_{32}, e_{33}]^T. \tag{13}$$

Essential matrix E is obtained by solving simultaneous equations for more than eight pairs of corresponding ray vectors. This means that we solve Eq. (14).

$$\min_{e} \|\mathbf{U}\mathbf{e}\|^2, \tag{14}$$

where $\mathbf{U} = [\mathbf{u}_1, \mathbf{u}_2, \cdots \mathbf{u}_n]^T$. Essential matrix E is obtained from e which is given as the eigenvector of the smallest eigenvalue of $\mathbf{U}^T \mathbf{U}$.
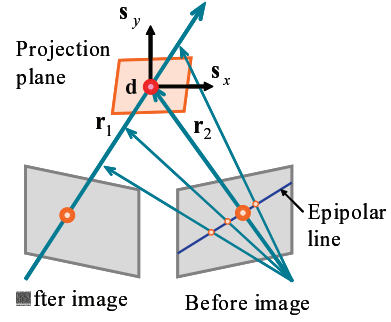
From essential matrix E, we calculate rotation matrix R and translation vector t. Essential matrix E is represented by rotation matrix R and translation vector $\mathbf{t} = [t_x, t_y, t_z]^T$.

$$\mathbf{E} = \mathbf{R}\mathbf{T}. \tag{15}$$

where

$$\mathbf{T} = \begin{bmatrix} 0 & -t_z & t_y \\ t_z & 0 & -t_x \\ -t_y & t_x & 0 \end{bmatrix}. \tag{16}$$

However, all feature points tracked along the image sequence do not behave as corresponding points because of image noise. Mistracked feature points should be rejected as outliers. To solve this problem, we employ RANSAC (RANdom SAmple Consensus) [23].

C. Re-Estimation of Camera Motion

The rotation matrix and the translation vector estimated in Section V-B may not be always good results because of various errors in images. Then, our method re-estimates the camera motion in consideration of the measurement errors in each feature point. Bundle adjustment [24] is used for re-estimation of the camera motion. The method minimizes the sum of feature re-projection errors which represents difference between the image coordinates of the original feature point and the reprojected point.
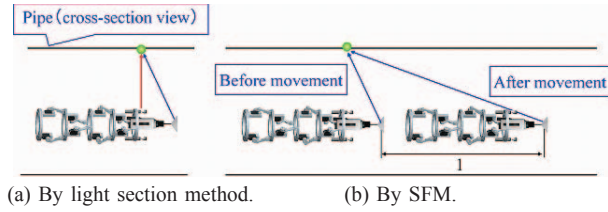
(a) By light section method.   (b) By SFM.

Fig. 15.   Scale matching.

Fig. 16.   Delaunay triangulation.

Fig. 17.   Experimental environment.   Fig. 18.   Protuberance.

D. Scale Matching

SFM cannot determine the distance $|\mathbf{t}|$ between two observation points because the measurement only uses images for input and does not get any scale information.

In our method, the 3-D coordinates of point measured by the light section method includes scale information. Therefore, we use the measurement result by the light section method for scale matching.

First, we measure the 3-D coordinates of a point by the light section method. The 3-D coordinates of the same point are measured by SFM (Fig. 15).

The ray vector is calculated from corresponding points. Since a feature point extracted by SIFT method is not always corresponds with a point measured by light section method, template matching is used for getting corresponding points (Perspective projection translation described in section V-A is performed in advance). Then, the 3-D coordinates of the point are given as those of the cross-point of two ray vectors.

Scale matching is realized by making the 3-D coordinates of the same point as close as possible. Minimization of deviation of the two resultant coordinates of the same point is more sensitive when the point lies farther from the observation point. Therefore it is appropriate to minimize the distances of coordinates. Scale l is calculated by Eq. (17).

$$\min \sum_{k=1}^{m} \| \log \mathbf{p}_k - \log l \mathbf{p}'_k \|, \tag{17}$$

where $\mathbf{p} = [x_k, y_k, z_k]^T$ represents the measurement result by the light section method, and $\mathbf{p}' = [x'_k, y'_k, z'_k]^T$ represents the measurement result by SFM, respectively. By the procedure, we can integrate the individual measurement data with matched scale.

VI. TEXTURE MAPPING

A triangular mesh (Fig. 16) is generated from integrated measurement data by using the 3-D Delaunay triangulation. However, the Delaunay triangulation generates a triangular mesh which contradicts a physical shape because the triangular mesh does not consider the shape of the measurement object.

Therefore, the triangular optimization method [25] is applied to the triangular mesh. The method adapts the triangular mesh to the physical shape by detecting a texture distortion. By texture mapping to the triangular mesh, a 3-D pipe model is constructed.
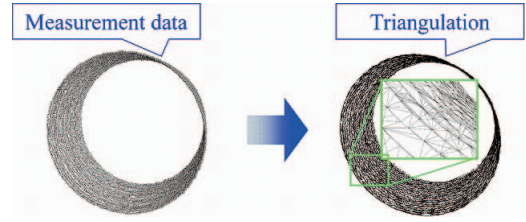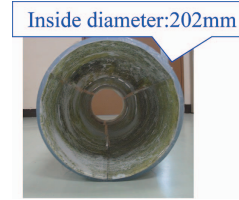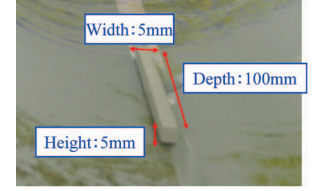
VII. EXPERIMENT

We used an IEEE-1394b camera GRAS-20S4C (Point Grey Research), and a hyperboloid mirror Hyper70 (Eizo). The image size is 1600×1200 pixels.

A pipe was prepared as a measurement object (Fig. 17). Assuming the case where the defects exist in the pipe, a protuberance was added to the pipe as shown in Fig. 18.

Figure 1 shows the earthworm robot equipped with the omni-directional range finder. The length of the robot is 520mm, and it is composed of four units (the inside diameter:100mm, the external diameter:150mm). The baseline between the omni-directional camera and the omni-directional laser is set to 82mm by the method described in chapter IV.

The laser light was emitted while the earthworm robot moved in the pipe. Then, the robot acquired an image sequence by using the omni-directional camera.

Figure 19 shows acquired image with LED illumination and without LED illumination.

Figure 20 shows the measurement result of pipe 3-D shape. Figure 20(a) is the bird's eye view of the experimental result. Figure 20(b) is the top view of the experimental result.

Table I shows comparison of the ground truth values and the measurement data. In Table I, the measurement value of the inside diameter is calculated by cylinder fitting. The measurement error of inside diameter is within 1mm and the average error is within the theoretical value 2mm. These results show that our proposed method can measure the pipe with high precision.

Figure 21 shows the experimental result of texture mapping. Figure 21(a) is the front view. Figure 21(b) is the internal view. The result shows the proposed method can measure the pipe in detail. By using texture information, recognition of the protuberance becomes easy.

VIII. CONCLUSION

In this paper, we propose a construction method of a 3-D pipe model by using an omni-directional range finder with a
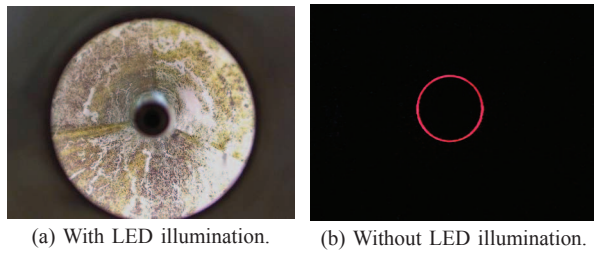
(a) With LED illumination.
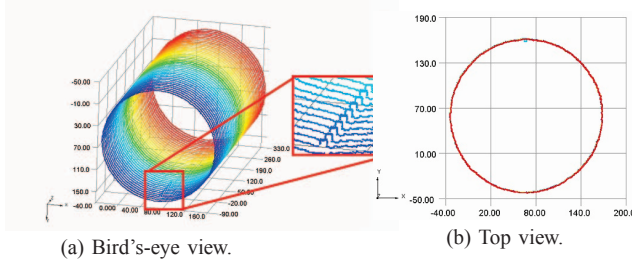

(b) Without LED illumination.

Fig. 19.   Aquired image.

(a) Bird's-eye view.

(b) Top view.

Fig. 20.   Result of 3-D shape measurement. [mm]

(a) Frontal view.

(b) Internal view.

Fig. 21.   Result of texture mapping.

TABLE I

ACCURACY EVALUATION.

	Measurement value	Ground truth
Inside diameter	203mm	202mm
Height of bulge	6mm	5mm
Width of bulge	6mm	5mm
Depth of bulge	102mm	100mm

light section method and SFM. Experimental results showed the effectiveness of the proposed method.

As a future work, an imperfection detection method should be considered.

REFERENCES

[1] H. B. Kuntze and H. Haffner: "Experiences with the Development of a Robot for Smart Multisensoric Pipe Inspection," *Proceedings of the 1998 IEEE International Conference on Robotics and Automation* (*ICRA1998*), pp.1773–1778, 1998.
[2] K. U. Scholl, V. Kepplin, K. Berns, and R. Dillmann: "Controlling a Multijoint Robot for Autonomous Sewer Inspection," *Proceedings of the 2000 IEEE International Conference on Robotics and Automation* (*ICRA2000*), pp.1701–1706, 2000.
[3] M. Horodinca, I. Doroftei and E. Mignon: "A Simple Architecture for In-Pipe Inspection Robots," *Proceedings of the 2002 International Colloquium on Mobile and Autonomous Systems*, pp.1–4, 2002.
[4] A. Zagler, and F. Pfeiffer: "MORITZ a Pipe Crawler for Tube Junctions," *Proceedings of the 2003 IEEE International Conference on Robotics and Automation* (*ICRA2003*), pp.2954–2959, 2003.
[5] A. Ahrary, A. A. F Nassiraei and M. Ishikawa: "A Study of An autonomous Mobile Robot for a Sewer Inspection System," *Journal of Artificial Life and Robotics*, Vol.11, No.1, pp.23–27, 2007.
[6] J. Gaspar, N. Winters and J. S. Victor: "Vision-Based Navigation and Environmental Representations with an Omnidirectional Camera," *IEEE Transactions on Robotics and Automation*, Vol.16, No.6, pp.890–898, 2000.
[7] Y. Yagi: "Omnidirectional Sensing and Its Applications," *IEICE Transactions on Information and Systems*, Vol.E82-D, No.3, pp.568–579, 1999.
[8] J. Gluckman and S. K. Nayar: "Ego-motion and Omnidirectional Cameras," *Proceedings of the 6th International Conference on Computer Vision* (*ICCV1998*), pp.999–1005, 1998.
[9] J. Kannala and S. S. Brandt and J. Heikkilä: "Measuring and Modelling Sewer Pipes from Video," *Machine Vision and Applications*, Vol.19, No.2, pp.73–83, 2008.
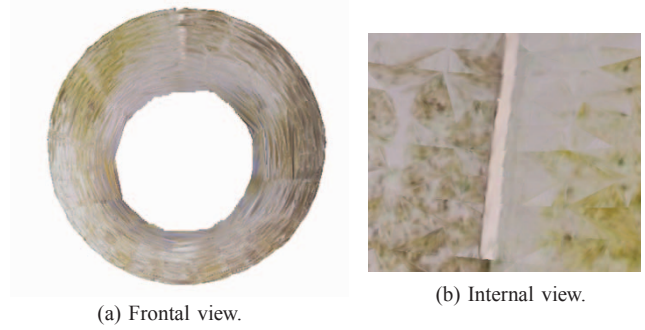[10] M. Kurisu, Y. Yokokohji, Y. Shiokawa and T. Samejima: "Development of a Laser Range. Finder for 3D Map-Building in Rubble," *Proceedings of the 2004 IEEE/RSJ International Conference on Intelligent Robots and Systems* (*IROS2004*), pp.443–448, 2004.
[11] M. Senoh, F. Kozawa and M. Yamada: "Development of Shape Measurement System Using an Omnidirectional Sensor and Light Sectioning Method with Laser Beam Scanning for Hume Pipes," *Optical Engineering*, Vol.45, No.6, pp.064301.1–064301.11, 2006.
[12] S. Yi, B. Choi, and N. Ahuja: "Real-time Omni-directional Distance Measurement with Active Panoramic Vision," *International Journal of Control, Automation, and Systems*, Vol.5, No.2, pp.184–191, 2007.
[13] R. Orghidan, E. Mouaddib, J. Salvi: "Omni-directional Depth Computation from a Single Image," *Proceedings of the 2005 IEEE International Conference on Robotics and Automation* (*ICRA2005*), pp.1234–1239, 2005.
[14] M. Tomono: "3-D Localization and Mapping Using a Single Camera Based on Structure-from-Motion with Automatic Baseline Selection," *Proceedings of the 2005 IEEE International Conference on Robotics and Automation* (*ICRA2005*), pp.3353–3358, 2005.
[15] B. Micusik and T. Pajdla: "Structure from Motion with Wide Circular Field of View Cameras," *IEEE Transactions on Pattern Analysis and Machine Intelligence*, Vol.28, No.7, pp.1135–1149, 2006.
[16] M. Lhuillier: "Automatic Scene Structure and Camera Motion using a Catadioptric System," *Computer Vision and Image Understanding*, Vol.109, No.2, pp.186–203, 2008.
[17] K. Matsui, A. Yamashita and T. Kaneko: "3-D Shape Measurement of Pipe by Range Finder Constructed with Omni-Directional Laser and Omni-Directional Camera," *Proceedings of the 2010 IEEE International Conference on Robotics and Automation* (*ICRA2010*), pp.2537–2542, 2010.
[18] N. Saga and T. Nakamura: "Elucidation of Propulsive Force of Micro-Robot Using Magnetic Fluid," *Journal of Applied Physics*, Vol.91, No.10, pp.7003–7005, 2002.
[19] T. Nakamura and T. Iwanaga: "Locomotion Strategy for a Peristaltic Crawling Robot in a 2-Dimensional Space," *Proceedings the 2008 IEEE International Conference on Robotics and Automation* (*ICRA2008*), pp.4361–4366, 2008.
[20] R. B. Fisher and D. K. Naidu: "A Comparison of Algorithms for Subpixel Peak Detection," *Proceedings of the 1991 British Machine Vision Association Conference*, pp.217–225, 1991.
[21] D. G. Lowe: " Distinctive Image Features from Scale-Invariant Keypoints," *International Journal of Computer Vision*, Vol.60, No.2, pp.91–110, 2004.
[22] R. Hartley: "In Defense of the Eight-Point Algorithm," *IEEE Transactions on Pattern Analysis and Machine Intelligence*, Vol.19, No.6, pp.580–593, 1997.
[23] M. A. Fischler and R. C. Bolles: "Random Sample Consensus: A Paradigm for Model Fitting with Applications to Image Analysis and Automated Cartography," *Communications of the ACM*, Vol.24, No.6, pp.381–395, 1981.
[24] B. Triggs, P. McLauchlan, R. Hartley and A. Fitzgibbon: "Bundle Adjustment - A Modern Synthesis," *Vision Algorithms:Theory & Practice, Springer-Verlag LNCS 1883*, 2000.
[25] A. Nakatsuji, Y. Sugaya and K. Kanatani: "Optimizing a Triangular Mesh for Shape Reconstruction from Images," *IEICE Transactions on Information and Systems*, Vol.E88-D, No.10, pp.2269–2276, 2005.